buildings

MDPI

Article

Influence of Compressive Strength of Concrete on Shear Strengthening of Reinforced Concrete Beams with Near Surface Mounted Carbon Fiber-Reinforced Polymer

Ma'en Abdel-Jaber [1], Mu'tasim Abdel-Jaber [2,†], Hasan Katkhuda [3,*], Nasim Shatarat [4] and Rola El-Nimri [4]

1 School of Construction Technology and Built Environment, Faculty of Engineering, Al Hussein Technical University, Amman 11183, Jordan; maen.abdel-jaber@htu.edu.jo
2 Department of Civil Engineering, Al-Ahliyya Amman University, Amman 19328, Jordan; m.abdeljaber@ammanu.edu.jo
3 Department of Civil Engineering, The Hashemite University, Zarqa 13133, Jordan
4 Department of Civil Engineering, The University of Jordan, Amman 11942, Jordan; n.shatarat@ju.edu.jo (N.S.); rola.elnimri@gmail.com (R.E.-N.)
* Correspondence: hasan@hu.edu.jo
† On sabbatical leave from Department of Civil Engineering, The University of Jordan, Amman 11942, Jordan.

Abstract: This paper investigates the effect of using near-surface mounted carbon fiber-reinforced polymer (NSM-CFRP) on the shear strengthening of rectangle beams with low strength concrete ($f'c$ = 17 MPa), medium strength concrete ($f'c$ = 32 MPa), and high strength concrete ($f'c$ = 47 MPa). The experimental program was performed by installing NSM-CFRP strips vertically in three different configurations: aligned with the internal stirrups, one vertical NSM-CFRP strip between every two internal stirrups, and two vertical NSM-CFRP strips between every two internal stirrups. All tested beams were simply supported beams and tested under a three-point loading test. The experimental results were compared with the theoretical capacities that were calculated according to the ACI 440.2R-17 and finite element analysis (FEA) that was conducted using ABAQUS software to simulate the behavior of all beams. The experimental results indicated that using NSM-CFRP limited the failure mode of all beams to pure shear failure with no debonding or rapture of the carbon strips. Moreover, the use of NSM-CFRP proved its efficiency by increasing the shear capacity of all beams by a range of 4% to 66%, in which the best enhancement was recorded for the case of using two unaligned NSM-CFRP strips. In general, the experimental shear capacities increased with the increase in the compressive strength of all beams. On the other hand, the ACI 440.2R-17 was conservative in predicting the theoretical shear capacities, and the FEA results agreed well with the experimental results.

Keywords: near-surface mounted; carbon fiber; concrete strength; finite element analysis

Citation: Abdel-Jaber, M.; Abdel-Jaber, M.; Katkhuda, H.; Shatarat, N.; El-Nimri, R. Influence of Compressive Strength of Concrete on Shear Strengthening of Reinforced Concrete Beams with Near Surface Mounted Carbon Fiber-Reinforced Polymer. *Buildings* **2021**, *11*, 563. https://doi.org/10.3390/buildings11110563

Academic Editors: Luís Filipe Almeida Bernardo and Miguel Nepomuceno

Received: 27 October 2021
Accepted: 19 November 2021
Published: 21 November 2021

1. Introduction

Reinforced concrete (RC) structures are widely used in construction; however, their performance is affected by several factors including the properties of the materials used and prevailing conditions. RC elements lose their strength due to aging, exposure to natural disasters, or faults in concrete production and construction [1–3]. Accordingly, the necessity to strengthen the RC elements before loading become an important aspect to allow existing structures to bear additional loads during their service life and to avoid any sudden failure, especially shear failure [4].

Fiber-reinforced polymer (FRP) materials have attracted attention for use in the strengthening and rehabilitation of RC elements in recent years. FRP is a material composed of polymers reinforced with different types of fibers [5]. This combination provides several advantages over other conventional construction materials, such as steel and wood.

FRP is known for its high strength, light weight, non-corrosiveness, ease of handling and installation, and the wide availability and diversity of all sizes, geometry, and dimensions [3]. There are different types of fibers; however, carbon, glass, and aramid are the types of FRPs that are the most widely used [5].

Two main techniques can be used to strengthen RC elements with FRPs: namely, externally bonded (EB) and near-surface mounted (NSM) techniques. The EB technique is applied by bonding the FRP sheets or laminates to the external faces of the RC element using high strength adhesives (epoxy resin or cement grout). Several studies were conducted on strengthening RC elements with EB carbon fiber-reinforced polymers (CFRP) in compression [6], flexure [7–9], and shear [10–28]. The main conclusions proved that using CFRP in the strengthening process enhanced the capacity of all elements; however, premature failure occurred extensively due to CFRP rapture and debonding. In shear strengthening, the EB technique was found to be effective in increasing the capacity using all schemes of sheets and laminates (horizontal, vertical, and inclined with different angles); however, the inclined CFRP laminates recorded better enhancement than other schemes [27,28]. Moreover, the larger the effective depth of the beam, the higher the chance of the CFRP debonding and propagation of shear cracks before failure [29].

The NSM technique was considered as a solution to delay the CFRP debonding due to the increased bond area between the concrete and CFRP faces [4]. This technique is applied by installing the FRP bars, ropes, or strips into precut open grooves in the concrete cover using epoxy or cement-based adhesives. This technique does not need any surface treatment or preparation other than grooving [30], and it lowers the damage resulting from fire, aging effects, and mechanical damages [31]. In 2009, Rizzo and Lorenzis [32] studied the behavior and capacity of RC beams strengthened with NSM CFRP. Round bars and strips were used with different spacing, inclination, and groove-filling epoxy resin. They concluded that the use of NSM-CFRP enhances the shear capacity; however, side concrete cover separation of the internal stirrups was noticed without CFRP debonding. Moreover, the stiffer the epoxy resin used, the lower the CFRP contribution to the shear capacity. In 2019, Al Rjoub et al. [33] investigated the effect of strengthening RC beams with NSM-CFRP in shear. The side concrete cover depth, NSM-CFRP inclination angle, and the length of the strips were tested. This study proved that longer and inclined strips are better than short and horizontal strips. In addition, concrete cover separation can be delayed or prevented by increasing the concrete cover depth. Saadah et al. [34] conducted a study to examine the behavior of RC beams strengthened with CFRP strips and ropes. Different spacings, inclination, and schemes were considered. The results indicated that inclined ropes and strips had the largest capacity depending on the spacing; the lower the spacing used, the larger the enhancement in capacity. Moreover, the use of NSM-CFRP ropes and strips changed the failure mode from brittle shear to flexural shear failure.

In this paper, set of tests was conducted to investigate the shear behavior of RC rectangle beams strengthened with NSM-CFRP vertical strips. The significance of this study comes from the fact that the NSM-CFRP configurations were chosen relative to the internal shear stirrups. Three different configurations were adopted: aligned with the internal stirrups, one vertical NSM-CFRP strip between every two internal stirrups, and two vertical NSM-CFRP strips between every two internal stirrups. Additionally, three different compressive strengths were considered, low strength concrete ($f'c$ = 17 MPa), medium strength concrete ($f'c$ = 32 MPa), and high strength concrete ($f'c$ = 47 MPa). All tested beams were simply supported beams and tested under a three-point loading test. The amount of the flexural steel was changed with changing the compressive strength to satisfy the amount of ρ_{max} to represent real designed cases. In addition, the experimental results are compared with the theoretical capacities predicted by the ACI 440.2R-17 [35] and finite element analysis (FEA) that was performed using ABAQUS software.

2. Experimental Investigation

2.1. Materials

2.1.1. Concrete

To investigate the effect of changing the compressive strength on the behavior of strengthened beams using NSM-CFRP, three compressive strengths were considered in this study to reflect the effect of using low strength concrete of 17 MPa, medium strength concrete of 32 MPa, and high strength concrete of 47 MPa. Six (150 mm × 150 mm × 150 mm) cubes were cast from each batch and tested to obtain the actual compressive strength at 28 days of casting. The average experimental compressive strengths after 28 days obtained were 15.62, 31.55, and 42.62 MPa for low, medium, and high strength concrete, respectively.

2.1.2. Steel

The longitudinal reinforcements used were high yield strength deformed bars with average ultimate and yield strength of 680 and 420 MPa, respectively. While the shear stirrups used were Φ8 mm mild steel bars with an average yield strength of 280 MPa.

2.1.3. Carbon Fiber Reinforced Polymer (CFRP)

Carbon fiber strips of 15 mm width and 2.5 mm thickness were used in this study. This type was supplied from the manufacturer in rolls (Figure 1) with the properties illustrated in Table 1.

Figure 1. Original carbon fiber roll.

Table 1. Technical data of CFRP.

Density	Glass Transition Temperature	Fiber Volume Content	E-Modulus (Mean Value)	Tensile Strength (Mean Value)	Strain at Break (Minimum Value)
1.60 g/cm^3	>100 °C	>68%	165,000 N/mm^2	3100 N/mm^2	>1.70%

2.1.4. Epoxy Resin

Two-part thixotropic epoxy resin (Sikadur-330) supplied from Sika company was used. Type A is the resin and type B is the hardener. Both types are made of paste with white and grey colors for part A and B, respectively. The materials were mixed in predefined proportions as provided by the manufacturer. Table 2 provides the technical data of the epoxy resin.

Table 2. Technical data of the epoxy resin.

Density	Thermal Expansion Coefficient	E-Modulus (Mean Value)	Tensile Strength (Mean Value)	Bond Strength	Elongation at Break
1.30 kg/L ± 0.1 kg/L (part A + B mixed)	4.5×10^{-5} per °C (−10 °C to +40 °C)	3800 N/mm^2 (7 days at +23 °C) / 4500 N/mm^2 (7 days at +23 °C)	30 N/mm^2 (7 days at +23 °C)	Concrete fracture (>4 N/mm^2) on sandblasted substrate	0.9% (7 days at +23 °C)

2.2. Beams Geometry and Reinforcement Details

A total of 12 beams, all having a length of 2000 mm and a cross-section of 300 mm × 200 mm (depth × width), were tested in this study with a concrete cover of 40 mm left on all sides. The beams were designed according to ACI 318-19 [36] to fail in shear. The amount of flexural steel was maintained constant among each group to satisfy the amount of ρ_{max}, in which the area of steel for beams with 17, 32, and 47 MPa compressive strength was 763.4, 1119.2, and 1472.6 mm^2, respectively. Then, Φ8 mm stirrups were installed at 350 mm with two additional stirrups located at both sides of each support. Figure 2 illustrates the beams' geometry and reinforcement details.

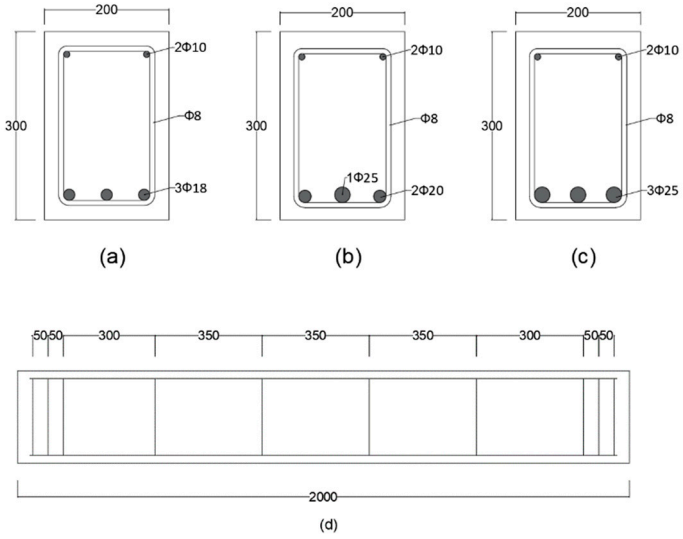

Figure 2. Beams' geometry: (**a**) cross-section of beams with 17 MPa, (**b**) cross-section of beams with 32 MPa, (**c**) cross-section of beams with 47 MPa, and (**d**) longitudinal section showing locations of internal stirrups (units: mm).

2.3. Details of Specimens

Specimens were divided into three groups according to the compressive strength used. Accordingly, group A represents the beams of low strength concrete, group B represents the beams with medium strength concrete, and group C represents the beams with high strength concrete. Each group consisted of four specimens divided as follows: one control beam that was tested without any NSM-CFRP attached, one beam having vertical strips of NSM-CFRP aligned with the internal stirrups, one beam having one vertical NSM-CFRP strip between every two internal stirrups, and one beam having two vertical NSM-CFRP strips between every two internal stirrups. Figure 3 illustrates the details of NSM-CFRP configurations.

The beams were named in the order of B—type of concrete—configuration of NSM-CFRP, in which B is designated for beam. The second term is for concrete strength, i.e., L is for low strength concrete, M for medium strength concrete, H is for high strength

concrete. The third term is for NSM-CFRP configurations, i.e., A is for aligned NSM-CFRP with internal stirrups, U1 is for one unaligned NSM-CFRP strip, and U2 is for two unaligned NSM-CFRP strips. For example, specimen BM-U1 refers to a beam with medium strength concrete (32 MPa) having one unaligned NSM-CFRP strip between any two internal stirrups.

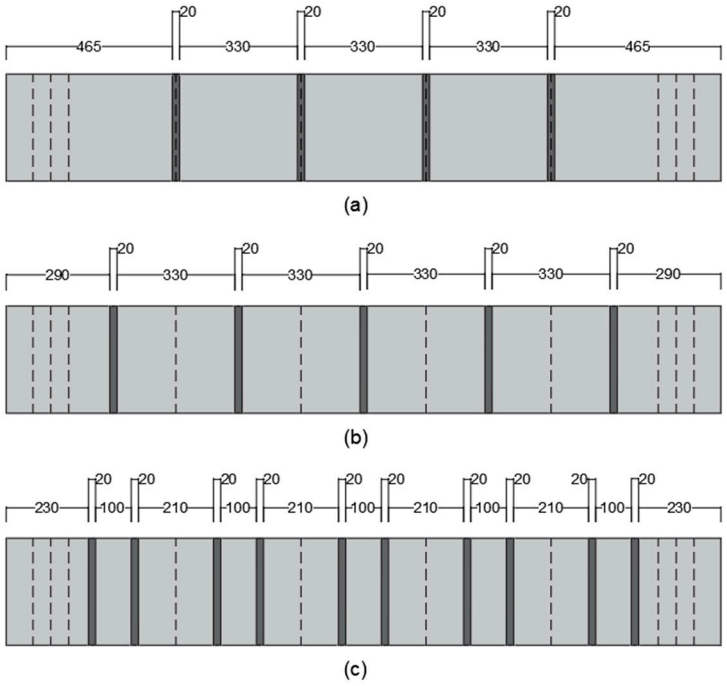

Figure 3. Details of NSM-CFRP configurations: (**a**) aligned NSM-CFRP, (**b**) one unaligned NSM-CFRP strip, and (**c**) two unaligned NSM-CFRP strips (units: mm).

2.4. Construction of Beams

2.4.1. Concrete Casting and Curing

The reinforcement steel was prepared according to the design, gathered, and fastened together using steel wires. After that, the reinforcement steel was lifted and placed in the formwork taking into account the concrete cover. The formwork was made from fairfaced wood to obtain a smooth and clean surface after casting without the need for any treatment. After the reinforcement steel was placed in the formwork, the concrete was poured and vibrated using a vibrating machine to eliminate any air bubbles and to prevent aggregates segregation. The beams were kept in the formwork for 21 days, and the curing process for 28 days was achieved by spraying water on the specimens.

2.4.2. CFRP Installation

The position of the required grooves was first defined on the surface of the beams with the required dimensions. The groove was 20 mm × 8 mm (width × thickness) that was made using an electric saw, and then an air blower was used to remove all the dust to ensure that the epoxy resin had a perfect bond with the concrete. The epoxy was mixed using a drill mixer and applied to the groove until its was partially filled. The carbon fiber was then placed into its position, and the surface was levelled by special instruments. The specimens were tested after one week of installing the NSM-CFRP, according to its technical instructions, so that the epoxy hardened and gained its strength. Figure 4 shows photos of preparation of grooves and NSM-CFRP installation.

(**a**) (**b**)

Figure 4. NSM-CFRP installation: (**a**) preparation of groove and (**b**) NSM-CFRP installation.

2.5. Test Setup

All beams were tested under three-point loading test using a 700 kN MFL Prüf-systeme Universal Testing Machine. All beams were considered as simply supported beams. One dial gage was placed at the mid span of the beam to measure the deflection during the test. Figure 5 shows the test setup of this study.

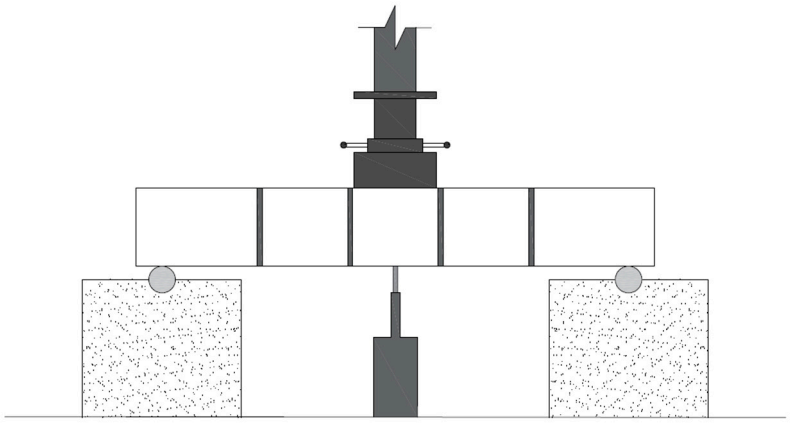

Figure 5. Test setup.

3. Theoretical Considerations

3.1. Theoretical Capacity According to the ACI 440.2R-17

The theoretical capacity of all beams was calculated according to ACI 440.2R-17 [35], which refers to the ACI 318-19 [36] in some terms. The code estimates the shear capacity by adding the contribution of concrete, reinforcement steel, and the NSM-CFRP together. The ACI code defines the theoretical shear strength as:

$$\varnothing V_n = \varnothing\left(V_c + V_s + \psi_f V_f\right), \quad (1)$$

where $\varnothing$ is a reduction factor and equals 0.75, V_n is the nominal shear strength of the beam, V_c is the nominal shear strength provided by concrete with steel flexural reinforcement, V_s is the nominal shear strength provided by steel stirrups, ψ_f is a strength reduction factor for NSM-CFRP, and V_f is the nominal shear strength provided by NSM-CFRP. The ACI 440.2R-17 [35] refers to the ACI 318-19 [36] with calculating the terms V_c and V_s.

3.2. Finite Element Analysis (FEA)

3.2.1. Parts

This model was constructed from two main groups: group 1 consisted of all parts that developed the main beams, and group 2 consisted of all parts that were needed to perform the test and simulate the actual setup. Group 1 contained the concrete, steel reinforcement,

and carbon fiber strips, while group 2 included supports and steel plates to apply the deflection. However, for beams strengthened with carbon fiber, grooves were made in the concrete part at the same location as in the actual beams to install the carbon fiber inside. Figure 6 shows the concrete with grooves for the unaligned scheme.

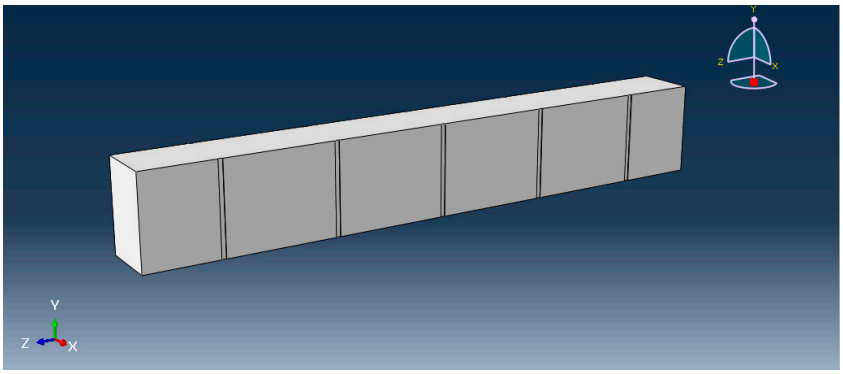

Figure 6. Concrete part for unaligned carbon fiber scheme.

3.2.2. Materials Definition

Reinforcement steel was defined as an elastic, perfectly plastic material with a Poisson's ratio of 0.3, while the concrete was defined as an elastic material with 0.2 Poisson's ratio. However, the plasticity of concrete, which plays a major role in the material properties, was defined using the concrete damage plasticity model (CDP) with plasticity parameter values obtained from ABAQUS user manual [37]. The input data were obtained using Tsai's equation [38] for the compressive behavior and Okamura's model [39] for the tension behavior with Tamai's proposed value [40]. Figure 7 illustrates the compressive and tensile stress–strain diagrams. The carbon fiber strips were defined as an elastic material with the actual properties provided by the manufacturer.

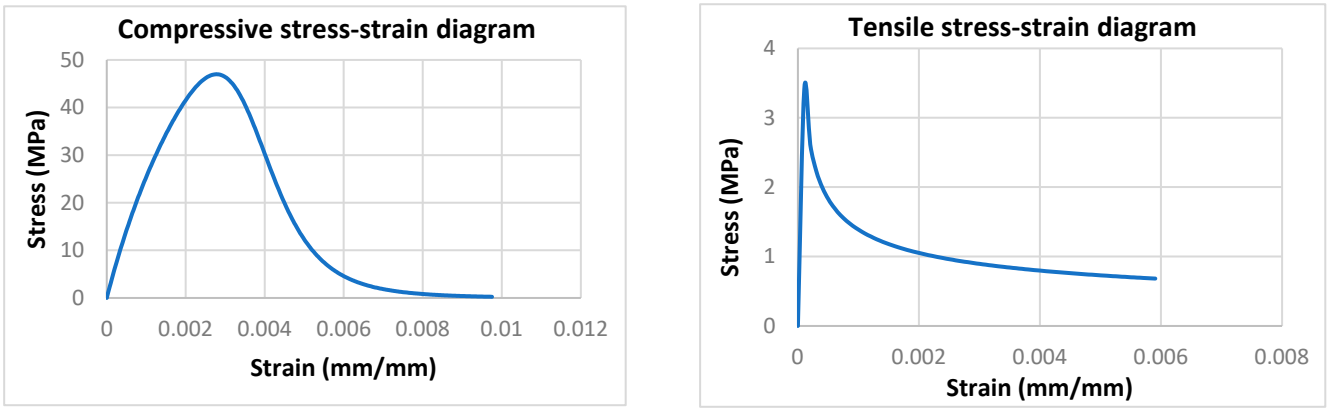

Figure 7. Compressive and tensile stress–strain diagrams for high strength concrete (f′c = 47 MPa).

3.2.3. Sections

The concrete section was defined as a solid homogeneous type, reinforcement steel was defined as a truss section to bear only axial forces, and the carbon fiber was defined as a shell homogeneous section. All sections were linked to one of the predefined materials before assigning them to the parts.

3.2.4. Meshing

The FE model was analyzed with three different mesh sizes of 50, 30, and 20 mm and two different mesh shapes of wedge and hexahedral types to determine the optimal mesh that provides low computational time with relatively accurate results before using the

appropriate mesh in the FE model presented in the manuscript. It was found that the size of the 30 mm mesh provided the most accurate results, since the 50 mm provided imprecise results, and the 20 mm recorded an anomaly response. Moreover, there was no significant difference between the response of the wedge-shaped model and the hexahedral-shaped model; thus, the hexahedral shape was selected because of its relatively small time to complete the job. After this small analysis, the concrete part was assigned to 3D stress family, steel reinforcement was assigned to truss family, and the carbon fiber was assigned to the shell family to keep them consistent with their parts' definition. After meshing, all parts were assembled in their place to obtain the final beam. Figure 8 shows the meshed beam from ABAQUS software.

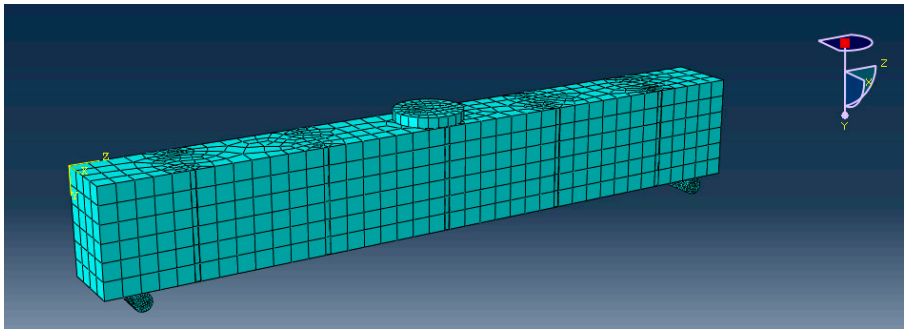

Figure 8. Meshing.

3.2.5. Interactions and Constraints

General contact interaction was assigned with a hard contact property and 0.3 friction coefficient between the beam and the setup parts to ensure the hard contact between the surfaces. Moreover, two constraints were defined. The steel reinforcement was embedded inside the concrete using the embedded region constraint, and the interaction between the concrete and the carbon was governed by using the tie constraint. The tie constraint was chosen because no debonding occurred during the test.

3.2.6. Boundary Conditions and Test Setup

One steel rod, located at 100 mm from each end of the beam, was defined as a pin support to perform the test. A dynamic explicit step was then created. A displacement control analysis was performed by applying the experimental displacement to the beam using a steel plate that was prohibited from moving in any direction except for the Y-direction (U2). The displacement was applied using a smooth step amplitude based on the step time that was changed to decrease the kinetic energy during the test.

4. Results and Discussion

4.1. General Behavior and Failure Modes

Upon the beginning of loading, flexural hair cracks started to appear on all specimens near the mid span at loads between 30 kN and 50 kN. With increasing the load, shear cracks were initiated near the support and propagated in an inclined path until they reached the loading point and caused the failure. All beams failed in shear; however, no debonding or CFRP rapture was noticed.

For beams with aligned NSM-CFRP strips, the shear cracks propagated behind the NSM-CFRP and changed its path in order to reach the loading point; thus, the inclination of the cracks was found to change between the two strips in which the crack propagated in between. Figure 9 shows the failure modes of beams with aligned NSM-CFRP strips.

(**a**)

(**b**)

(**c**)

Figure 9. Failure modes of beams with aligned NSM-CFRP strips: (**a**) BL-A, (**b**) BM-A, and (**c**) BH-A.

For beams with one unaligned NSM-CFRP strip between any two internal stirrups, the shear crack did not start until after the first NSM-CFRP strip. However, after the shear crack appeared, the same behavior as the beams with aligned NSM-CFRP strips was observed, and the cracks propagated behind the NSM-CFRP strips to reach the loading point. As mentioned before, the inclination of the cracks changed since the NSM-CFRP strips interrupted the cracks while propagating. Figure 10 shows the failure modes of beams with one unaligned NSM-CFRP strip between the internal stirrups.

(**a**)

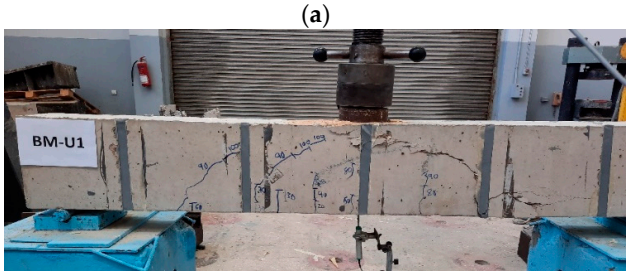

(**b**)

Figure 10. *Cont.*

(**c**)

Figure 10. Failure modes of beams with one unaligned NSM-CFRP strip: (**a**) BL-U1, (**b**) BM-U1, and (**c**) BH-U1.

For beams with the two unaligned NSM-CFRP strips pattern, the same failure modes and observations were recorded for all beams as mentioned before. Moreover, wider cracks and cover separation were noticed during the test. Figure 11 shows the failure modes of beams with two unaligned NSM-CFRP strips between the internal stirrups.

(**a**)

(**b**)

(**c**)

Figure 11. Failure modes of beams with two unaligned NSM-CFRP strips: (**a**) BL-U2, (**b**) BM-U2, and (**c**) BH-U2.

4.2. Experimental Load-Deflection Curves

The deflection of all beams was measured using a dial gage placed at the mid span of the beam. Figure 12 shows the experimental load-deflection curves for all compressive strengths. All beams contained NSM-CFRP showed almost the same load-deflection behavior. The beams containing NSM-CFRP with the same compressive strength showed higher deflection values than the control beam, which indicates that the NSM-CFRP increased the ductility of beams.

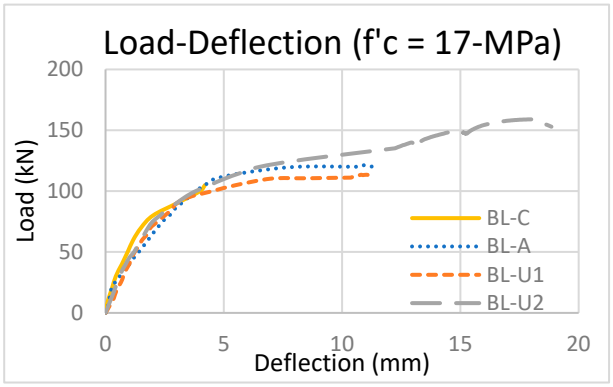

(**a**)

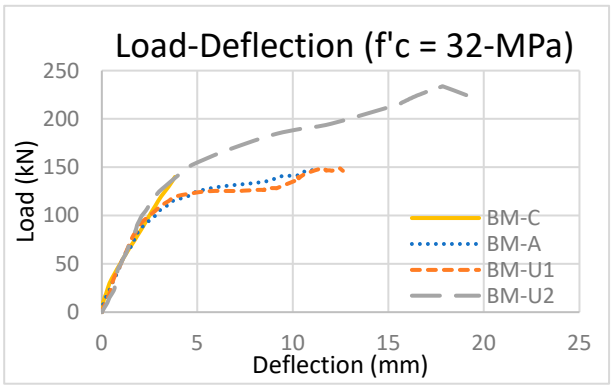

(**b**)

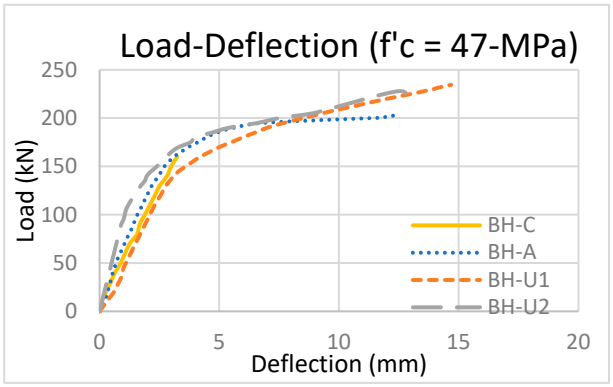

(**c**)

Figure 12. Experimental load-deflection curves: (**a**) low strength concrete, (**b**) medium strength concrete, and (**c**) high strength concrete.

The deflection along the beams' length was also plotted in Figure 13. It is noted that beams with low compressive strength that contain NSM-CFRP strips in any configuration recorded higher deflection values than the control beams including the high strength concrete. This also indicated that the use of the NSM-CFRP enhanced the ductility of beams.

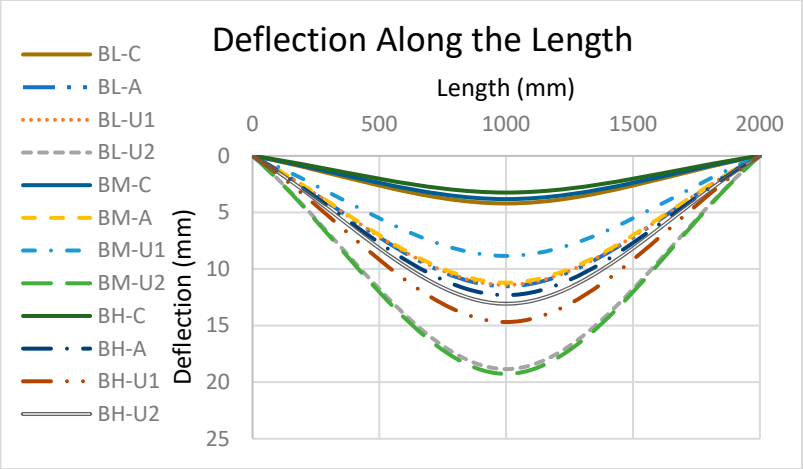

Figure 13. Deflection along the beams' length.

4.3. Experimental Ultimate Loads

All beams recorded a failure in shear. Table 3 shows the experimental capacities for all specimens. The percent increase in the table is with respect to the control beam in each group.

Table 3. Experimental load results.

Sample		Experimental Load (kN)	Percent Increase (%)
Low Strength Concrete	BL	105.0	-
	BL-A	121.3	16%
	BL-U1	113.4	8%
	BL-U2	158.9	51%
Medium Strength Concrete	BM	141.0	-
	BM-A	147.0	4%
	BM-U1	149.4	6%
	BM-U2	233.8	66%
High Strength Concrete	BH	168.4	-
	BH-A	202.8	20%
	BH-U1	234.5	39%
	BH-U2	228.7	36%

All beams strengthened with NSM-CFRP recorded higher load values when compared to the control beam. It can be seen that beams with aligned strips recorded the lowest enhancement in all groups; this can be attributed to the fact that the alignment of both the strips and the stirrups did not introduce a new level of reinforcement that would interrupt the shear cracks while propagating. The highest enhancement was recorded for beams with two NSM-CFRP strips unaligned with the shear stirrups, in which an enhancement of 66% was achieved for specimen BM-U2. For low strength concrete, medium strength concrete, and high strength concrete, the enhancement was in a range of 8–51%, 4–66%, and 20–39%, respectively.

For beams strengthened with the same NSM-CFRP scheme, it can be seen from Figure 14 that, in general, the shear capacity increased with the increase of the compressive strength used. This is due to the fact that the concrete carries part of the shear load, and its resistance increases with the increase of the compressive strength.

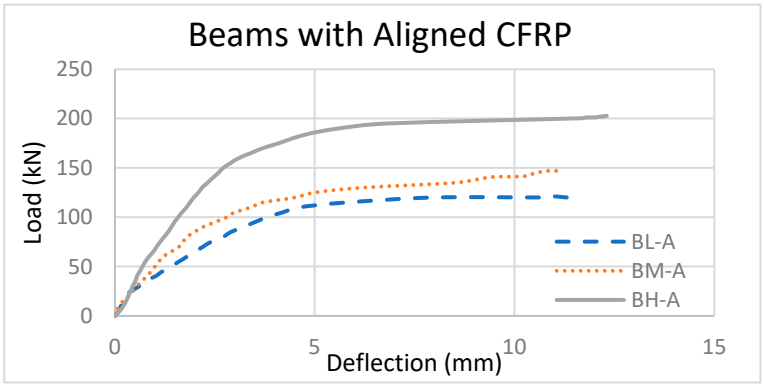

(**a**)

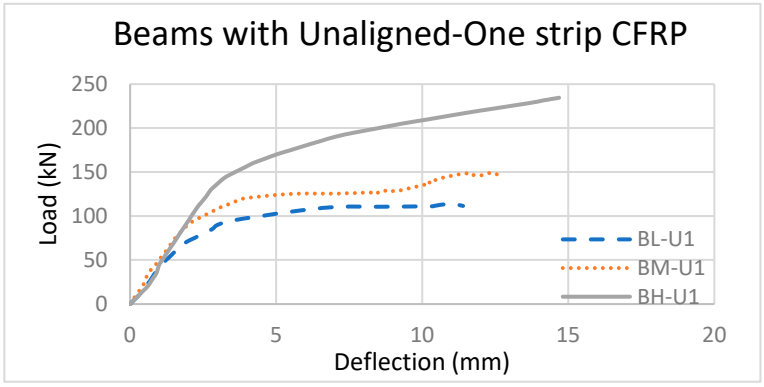

(**b**)

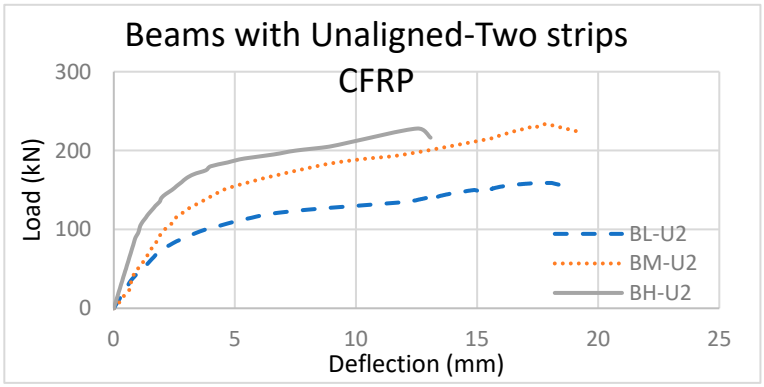

(**c**)

Figure 14. Comparison between beams with the same NSM-CFRP configuration: (**a**) aligned, (**b**) unaligned one strip, and (**c**) unaligned two strips.

4.4. Theoretical Results

Theoretical capacities were predicted using the ACI 440.2R-17 code [35] as mentioned before. Table 4 shows a comparison between the experimental and theoretical results.

It can be noted that the ACI 440.2R-17 [35] was conservative in predicting the theoretical capacities of all beams with different NSM-CFRP schemes. The experimental values were higher than the theoretical ones by a range of 23.2–50.9%. The ACI 440.2R-17 [35] did not consider the effect of the alignment between the stirrups and the NSM-CFRP; thus, the theoretical results of both schemes with an equal number of strips per spacing are the same. This does not agree well with the experimental results, as the difference between the aligned scheme and unaligned scheme with one strip ranges from 1.6% to 15.6%. Thus, the effect of the alignment should be considered in the codes' equations.

Table 4. Experimental and theoretical capacity results.

Sample		Experimental Shear Load (kN)	Theoretical Load (kN)	Percent Increase (%)
Low Strength Concrete	BL	52.5	40.3	23.2
	BL-A	60.6	42.5	29.9
	BL-U1	56.7	42.5	25.0
	BL-U2	79.5	43.3	45.5
Medium Strength Concrete	BM	70.5	52.6	25.5
	BM-A	73.5	56.1	23.7
	BM-U1	74.7	56.1	24.9
	BM-U2	116.9	57.3	50.9
High Strength Concrete	BH	84.2	58.5	30.5
	BH-A	101.4	62.8	38.0
	BH-U1	117.2	62.8	46.4
	BH-U2	114.3	64.4	43.7

Moreover, the contribution of double unaligned NSM-CFRP strips according to the code was very small; however, this was not the case in the experimental results. According to the code, the enhancement was 7%, 9%, and 10% for low strength, medium strength, and high strength concrete, respectively, while the actual enhancement was 51%, 66%, and 36% for low strength, medium strength, and high strength concrete, respectively.

4.5. FEA Results

The FEA results showed good agreement with the experimental ones concerning the maximum capacities and crack patterns. Figure 15 illustrates the maximum principal plastic strain for beam BM-A as an example. The maximum plastic strain indicates the cracks that occurred in concrete based on the material's definition (stress–strain relationship). It can be seen from the figure that the cracks occurred at the same location in the beam, and they changed their inclination between the carbon strips, which is the same pattern as the experimental one.

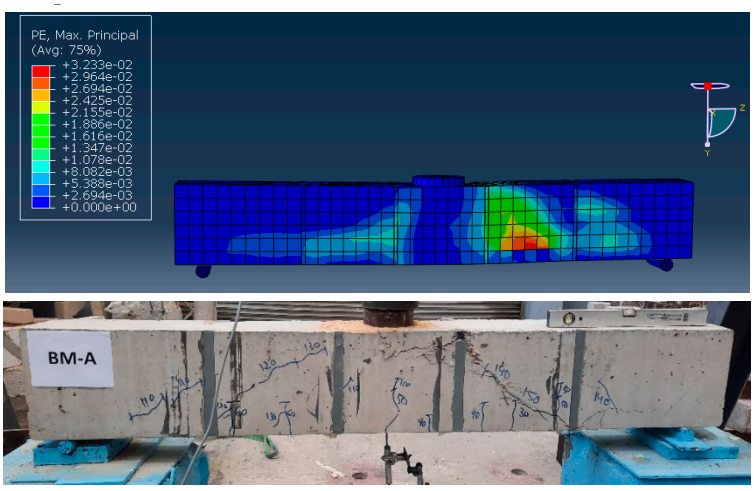

Figure 15. Maximum principal plastic strain for BM-A.

All beams analyzed using ABAQUS software showed nearly the same deflected shape as the experimental ones. Figure 16 shows the deflected shape for beam BL-U1.

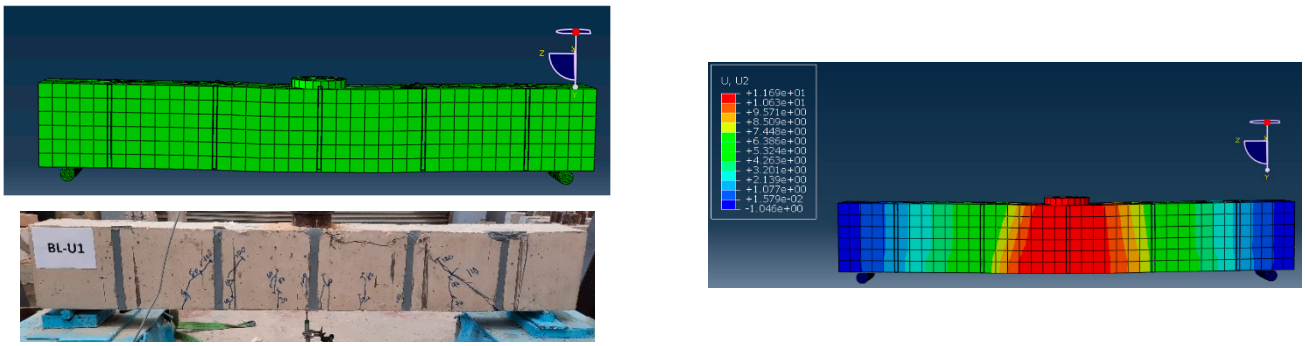

(**a**) (**b**)

Figure 16. (**a**) Experimental and FEA deflected shape and (**b**) deflection values.

Figure 17 shows a comparison of the load-deflection behavior between ABAQUS and the experimental results for all beams. It can be noted that all beams showed similar load deflection behavior until they reached the maximum load; however, some beams exhibited different behavior after reaching the maximum load than the experimental ones, especially the beams of high strength concrete strengthened with NSM-CFRP.

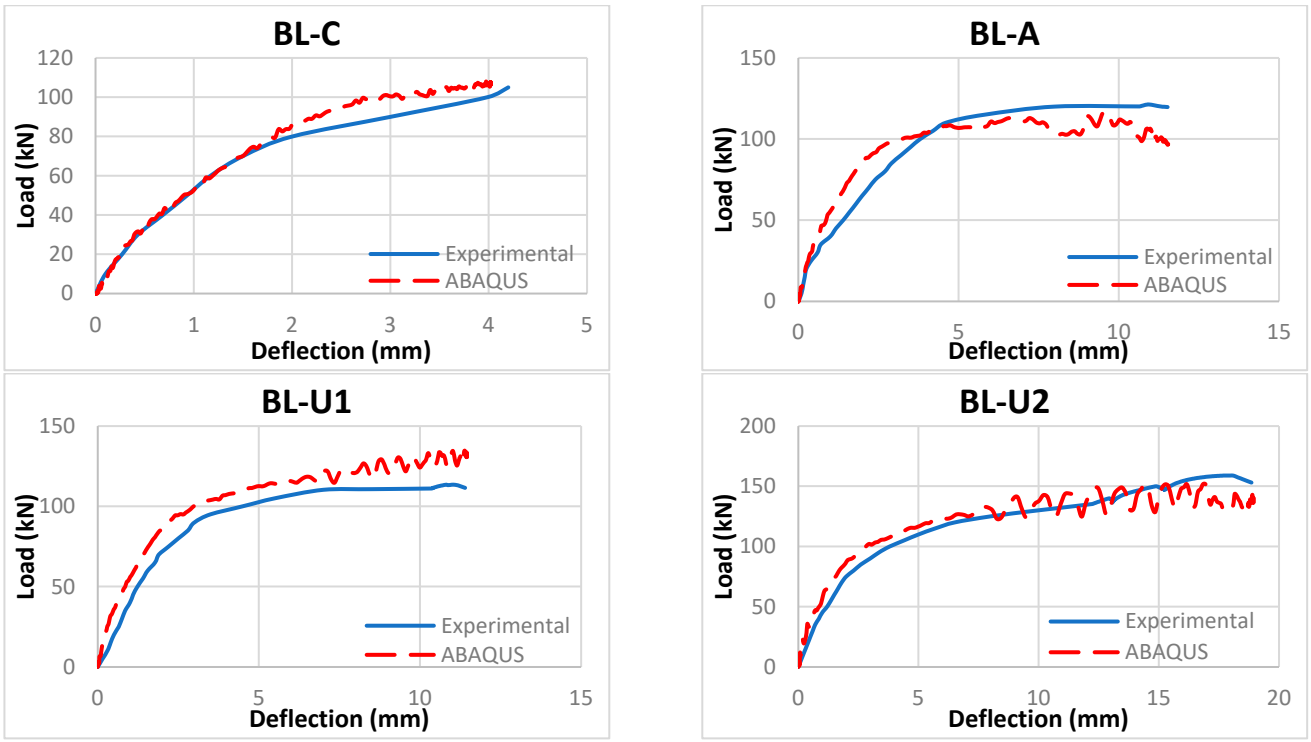

(**a**)

Figure 17. *Cont.*

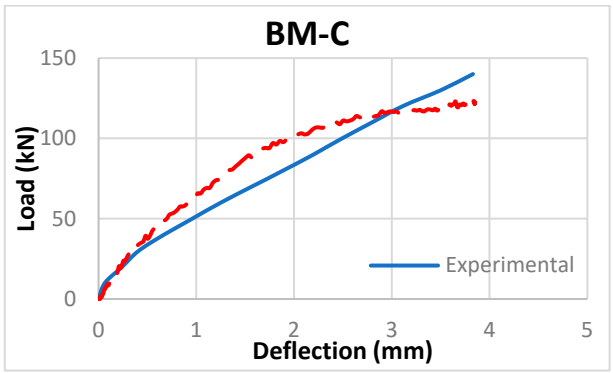

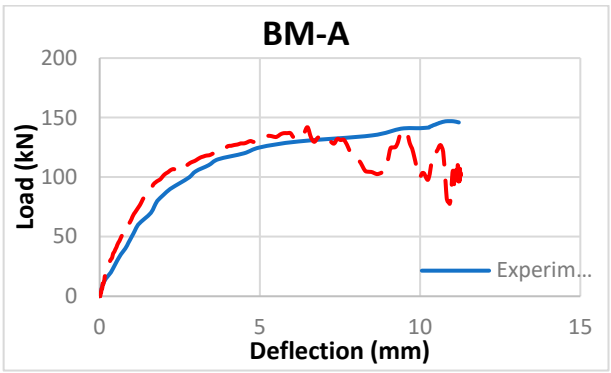

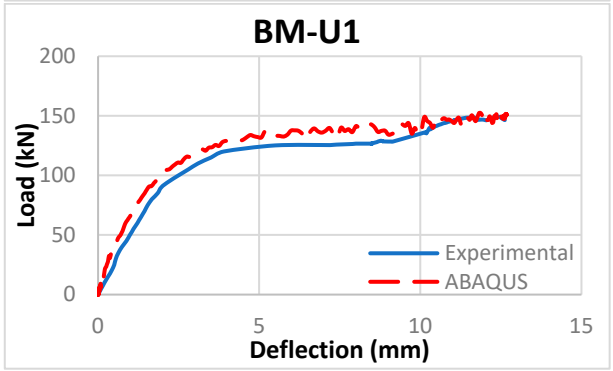

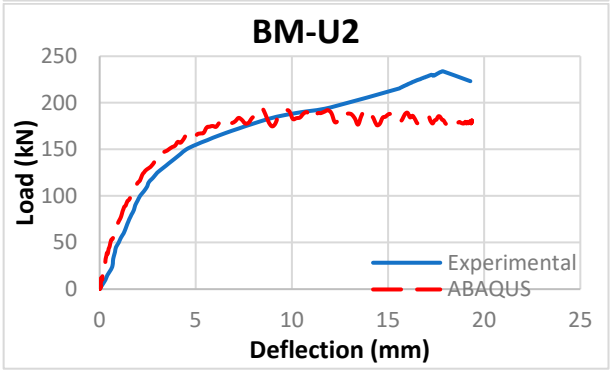

(**b**)

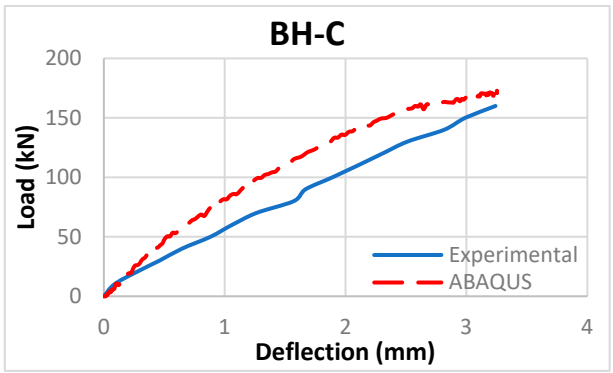

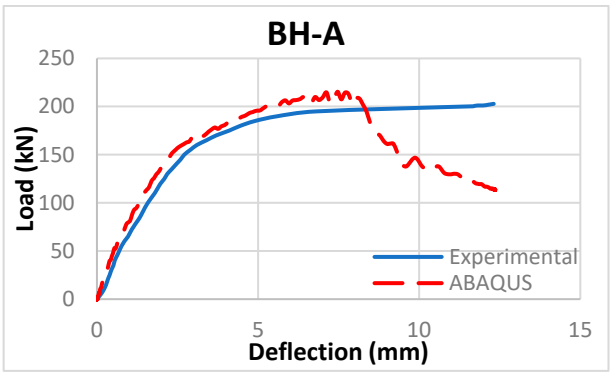

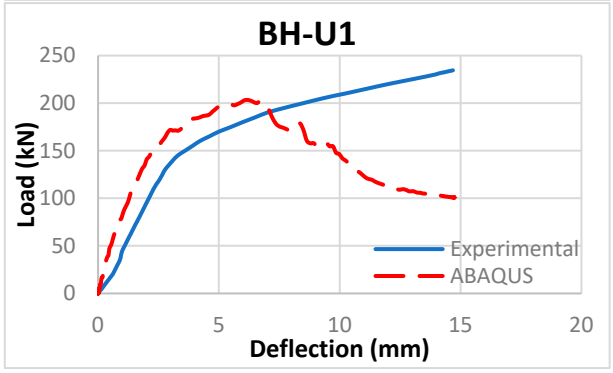

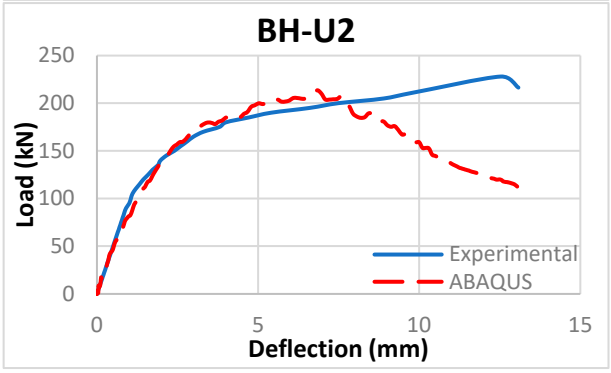

(**c**)

Figure 17. Comparison between the experimental and ABAQUS load-deflection behavior: (**a**) low strength concrete, (**b**) medium strength concrete, and (**c**) high strength concrete.

5. Conclusions

This study presents an experimental, theoretical, and numerical investigation of strengthening reinforced concrete beams with different concrete compressive strengths and NSM-CFRP configurations. From this study, the following can be concluded:

1. The use of NSM-CFRP limited the failure modes of the beams to pure shear failure, in which no debonding or CFRP rapture was noticed during the test.
2. The start, propagation, and inclination of the shear cracks depend on the NSM-CFRP scheme used. The shear cracks initiated after the first vertical NSM-CFRP strip if it was close to the support and changed its inclination between any two strips to reach the top face of the beam near the loading point.
3. Experimental load-deflection curves indicated that beams with NSM-CFRP attached have higher ductility than their corresponding control beams as they recorded higher deflection values.
4. In general, the experimental shear capacity increased with the increase of the compressive strength used for all beams strengthened with the same NSM-CFRP configuration.
5. The experimental shear capacity of all beams strengthened with NSM-CFRP was higher than their corresponding control beams, in which the enhancement in shear capacity was in a range of 4–66%. The highest enhancement was recorded for beams with the unaligned two NSM-CFRP strips pattern, followed by the unaligned one NSM-CFRP strip pattern and then the aligned strips.
6. The ACI 440.2R-17 was found to be conservative and predicted lower capacities than the experimental ones. However, the effect of the alignment between the NSM-CFRP strips and internal shear stirrups, as well as the number of unaligned NSM-CFRP strips, were not taken into consideration; thus, the theoretical values and enhancement percentages did not match the experimental results. As a result, the code equations for the shear design of NSM-CFRP should be adjusted to consider these factors to obtain more accurate capacities.
7. The FEA showed acceptable results with respect to the crack patterns and maximum load capacities.

Author Contributions: Conceptualization, M.A.-J. (Ma'en Abdel-Jaber) and M.A.-J. (Mu'tasim Abdel-Jaber); methodology, M.A.-J. (Mu'tasim Abdel-Jaber) and H.K.; software, R.E.-N.; validation, M.A.-J. (Ma'en Abdel-Jaber) and H.K.; formal analysis, N.S.; investigation, R.E.-N.; resources, M.A.-J. (Mu'tasim Abdel-Jaber); data curation, M.A.-J. (Ma'en Abdel-Jaber); writing—original draft preparation, R.E.-N.; writing—review and editing, H.K.; visualization, N.S.; supervision, M.A.-J. (Ma'en Abdel-Jaber) and M.A.-J. (Mu'tasim Abdel-Jaber); project administration, M.A.-J. (Mu'tasim Abdel-Jaber) and H.K.; funding acquisition, R.E.-N. All authors have read and agreed to the published version of the manuscript.

Funding: This research did not receive any specific grant from any funding agencies.

Institutional Review Board Statement: Not applicable.

Informed Consent Statement: Informed consent was obtained from all subjects involved in the study.

Data Availability Statement: All data of this research were presented in the article.

Conflicts of Interest: The authors declare no conflict of interest.

References

1. Islam, A.A. Effective methods of using CFRP bars in shear strengthening of concrete girders. *Eng. Struct.* **2009**, *31*, 709–714. [CrossRef]
2. Rahal, K.N.; Rumaih, H.A. Tests on reinforced concrete beams strengthened in shear using near surface mounted CFRP and steel bar. *Eng. Struct.* **2011**, *33*, 53–62. [CrossRef]
3. Dias, S.J.; Barros, J.A. Shear strengthening of RC T-beams with low strength concrete using NSM CFRP laminates. *Cem. Concr. Compos.* **2011**, *33*, 334–345. [CrossRef]

4. Jumaat, M.Z.; Shukri, A.A.; Obaydullah, M.; Huda, M.; Hosen, M.; Hoque, N. Strengthening of RC Beams Using Externally Bonded Reinforcement Combined with Near-Surface Mounted Technique. *Polymers* **2016**, *8*, 761.
5. Obaidat, Y.T.; Barham, W.S.; Aljarah, A.H. New anchorage technique for NSM-CFRP flexural strengthened RC beam using steel clamped end plate. *Constr. Build. Mater.* **2020**, *263*, 120246. [CrossRef]
6. Abed, D.J.; Nasim, M.S.; Shatarat, K. Behavior of Square Reinforced- Concrete Columns Strengthened with Carbon Fiber Reinforced Polymers (Cfrp) Under Eccentric Loading. *Int. J. Civ. Eng. Technol.* **2018**, *9*, 532–547.
7. Dong, J.; Wang, Q.; Guan, Z. Structural Behavior of RC Beams with External Flexural and Flexural–Shear Strengthening by FRP Sheets. *Compos. Part B* **2013**, *44*, 604–612. [CrossRef]
8. Al-Ghanim, H.; Al-Asi1, A.; Abdel-Jaber, M.; Alqam, M. Shear and Flexural Behavior of Reinforced Concrete Deep Beams Strengthened with CFRP Composites. *Mod. Appl. Sci.* **2017**, *10*, 110–122. [CrossRef]
9. Hassan, S.K.; Abdel-Jaber, M.S.; Alqam, M. Rehabilitation of Reinforced Concrete Deep Beams Using Carbon Fiber Reinforced Polymers (CFRP). *Mod. Appl. Sci.* **2018**, *12*, 179–194. [CrossRef]
10. Chajes, M.J.; Januska, T.F.; Mertz, D.R.; Thomson, T.A.; Finch, W.W. Shear Strengthening of Reinforced Concrete Beams Using Externally Applied Composite Fabrics. *ACI Struct. J.* **1995**, *92*, 295–303.
11. Triantafillou, T.C. Shear Strengthening of Reinforced Concrete Beams Using Epoxy-Bonded FRP Composites. *ACI Struct. J.* **1998**, *95*, 107–115.
12. Abdel-Jaber, M. Shear Strengthening of Reinforced Concrete Beams Using Externally Bonded Carbon Fibre Reinforced Plates. Ph.D. Thesis, Oxford Brookes University, Oxford, UK, 2001.
13. Teng, J.G.; Smith, S.T.; Yao, J.; Chen, J.F. Intermediate Crack-induced De-bonding in RC Beams and Slabs. *Constr. Build. Mater.* **2003**, *17*, 447–462. [CrossRef]
14. Abdel-Jaber, M.S.; Walker, P.R.; Hutchinson, A.R. Shear Strengthening of Reinforced Concrete Beams Using Different Configurations of Externally Bonded Carbon Fibre Reinforced Plates. *Mater. Struct. J.* **2003**, *36*, 291–301. [CrossRef]
15. Chen, J.F.; Tengb, J.G. Shear Capacity of FRP-Strengthened RC Beams: FRP Debonding. *Constr. Build. Mater.* **2003**, *17*, 27–41. [CrossRef]
16. Bousselham, A.; Chaallal, O. Shear Strengthening Reinforced Concrete Beams with Fiber-Reinforced Polymer: Assessment of Influencing Parameters and Required Research. *ACI Struct. J.* **2004**, *101*, 219–227.
17. Zhang, Z.; Hsu, C.T. Shear Strengthening of Reinforced Concrete Beams Using Carbon-Fiber-Reinforced Polymer Laminates. *J. Compos. Constr.* **2005**, *9*, 158–169. [CrossRef]
18. Adhikary, B.B.; Mutsuyoshi, H. Shear Strengthening of Reinforced Concrete Beams Using Various Techniques. *Constr. Build. Mater.* **2006**, *20*, 366–373. [CrossRef]
19. Abdel Hafez, A. Shear Behavior of RC Beams Strengthened Externally with Bonded CFRP–U Strips. *J. Eng. Sci.* **2007**, *35*, 361–379. [CrossRef]
20. Abdel-Jaber, M.S.; Shatanawi, A.S.; Abdel-Jaber, M.S. Guidelines for Shear Strengthening of Beams Using Carbon Fiber-Reinforced Polymer (FRP) Plates. *Jordan J. Civ. Eng.* **2007**, *1*, 327–335.
21. Barros, J.A.; Dias, S.J.; Lima, J.L. Efficacy of CFRP-based Techniques for the Flexural and Shear Strengthening of Concrete Beams. *Cem. Concr. Compos.* **2007**, *29*, 203–217. [CrossRef]
22. Al-Tersawy, S. Effect of Fiber Parameters and Concrete Strength on Shear Behavior of Strengthened RC Beams. *Constr. Build. Mater.* **2013**, *44*, 15–24. [CrossRef]
23. Imran, M.; Shafiq, N.; Akbar, I. Strengthening Techniques & Failure Modes of RC Beam Strengthened Using Fibre Reinforced Polymer. A Review. *GSTF J. Eng. Technol.* **2013**, *2*, 93–98.
24. Mostofinejad, D.; Hosseini, S.A.; Razavi, S.B. Influence of Different Bonding and Wrapping Techniques on Performance of Beams Strengthened in Shear Using CFRP Reinforcement. *Constr. Build. Mater.* **2016**, *116*, 310–320. [CrossRef]
25. Ibrahim, A.M.; Mansor, A.A.; Hameed, M. Structural Behavior of Strengthened RC Beams in Shear using CFRP Strips. *Open Civ. Eng. J.* **2017**, *11*, 205–215. [CrossRef]
26. Mhanna, H.H.; Hawilehb, R.A.; Abdallac, J.A. Shear Strengthening of Reinforced Concrete Beams Using CFRP Wraps. *Procedia Struct. Integr.* **2019**, *17*, 214–221. [CrossRef]
27. Bukhari, I.A.; Vollum, R.L.; Ahmad, S.; Sagaseta, J. Shear Strengthening of Reinforced Concrete beams with CFRP. *Mag. Concr. Res.* **2010**, *62*, 65–77. [CrossRef]
28. Alsayed, S.H.; Siddiqui, N.A. Reliability of Shear-Deficient RC Beams Strengthened with CFRP-Strips. *Constr. Build. Mater.* **2013**, *42*, 238–247. [CrossRef]
29. Godat, A.; Qu, Z.; Lu, Z.X.; Labossiere, P.; Ye, L.P.; Neale, K.W. Size Effects for Reinforced Concrete Beams Strengthened in Shear with CFRP Strips. *J. Compos. Constr.* **2010**, *14*, 260–271. [CrossRef]
30. De Lorenzis, L.; Teng, J.G. Near-Surface Mounted FRP Reinforcement: An emerging technique for strengthening structures. *Compos. Part B* **2007**, *38*, 119–143. [CrossRef]
31. Sena-Cruz, J.M.; Barros, J.A.O. Bond between near-surface mounted CFRP laminate strips and concrete. *J. Compos. Constr. ASCE* **2004**, *8*, 519–527. [CrossRef]
32. Rizzo, A.; De Lorenzis, L. Behavior and capacity of RC beams strengthened in shear with NSM FRP reinforcement. *Construct. Build. Mater.* **2009**, *23*, 1555–1567. [CrossRef]

33. Rjoub, Y.S.A.; Ashteyat, A.M.; Obaidat, Y.T.; Bani, S.Y. Shear strengthening of RC beams using near-surface mounted carbon fibre-reinforced polymers. *Aust. J. Struct. Eng.* **2019**, *20*, 54–62. [CrossRef]
34. Saadah, M.; Ashteyat, A.; Murad, Y. Shear strengthening of RC beams using side near surface mounted CFRP ropes and strips. *Structures* **2021**, *32*, 380–390. [CrossRef]
35. *ACI 440.2R-17, Guide for the Design and Construction of Externally Bonded FRP Systems for Strengthening Concrete Structures, Reported by ACI Committee 440*; ACI Committee: SanBernardino, CA, USA, 2017.
36. *ACI 318. '318M–19: Building Code Requirements for Reinforced Concrete and Commentary'*; ACI Committee: SanBernardino, CA, USA, 2019; p. 261.
37. ABAQUS User's Manual. 2008. Available online: http://130.149.89.49:2080/v6.14/books/usb/default.htm (accessed on 18 November 2021).
38. Tsai, W.T. Uniaxial compressional stress-strain relation of concrete. *J. Struct Eng.* **1988**, *114*, 2133–2136. [CrossRef]
39. Okamura, H.; Maekawa, K.; Sivasubramaniyam, S. Verification of modeling for reinforced finite element. In *Finite Element Of Reinforced Concrete Structures*; ASCE: Reston, VA, USA, 1985; pp. 528–543.
40. Tamai, S.; Shima, H.; Izumo, J.; Okamura, H. Average stress strain relationship in post yield range of steel bar in concrete. *Concr. Lib. JSCE* **1988**, *11*, 117–129.